AGU PUBLICATIONS

Water Resources Research

RESEARCH ARTICLE

10.1002/2013WR014610

Critical Reynolds number for nonlinear flow through rough-walled fractures: The role of shear processes

Morteza Javadi[1], Mostafa Sharifzadeh[1,2], Kourosh Shahriar[1], and Yasuhiro Mitani[3]

[1]Department of Mining and Metallurgical Engineering, Amirkabir University of Technology, Tehran, Iran, [2]Western Australian School of Mine, Curtin University, Kalgoorlie, Western Australia, Australia, [3]Institute of Environmental Systems, Kyushu University, Fukuoka, Kyushu, Japan

Key Points:
- A criterion for flow nonlinearity (CFN model) was developed for rock fractures
- Critical Reynolds number was defined based on the CFN model and Forchheimer's law
- The role of shearing on critical Reynolds number was experimentally investigated

Correspondence to:
M. Sharifzadeh,
M.Sharifzadeh@curtin.edu.au

Citation:
Javadi, M., M. Sharifzadeh, K. Shahriar, and Y. Mitani (2014), Critical Reynolds number for nonlinear flow through rough-walled fractures: The role of shear processes, *Water Resour. Res.*, *50*, 1789–1804, doi:10.1002/2013WR014610.

Received 19 AUG 2013
Accepted 28 JAN 2014
Accepted article online 6 FEB 2014
Published online 28 FEB 2014

Abstract This paper experimentally investigates the role of shear processes on the variation of critical Reynolds number and nonlinear flow through rough-walled rock fractures. A quantitative criterion was developed to quantify the onset of nonlinear flow by comprehensive combination of Forchheimer's law and Reynolds number. At each shear displacement, several high-precision water flow tests were carried out with different hydraulic gradients then the critical Reynolds number was determined based on the developed criterion. The results show that (i) the Forchheimer's law was fitted very well to experimental results of nonlinear fluid flow through rough-walled fractures, (ii) the coefficients of viscous and inertial pressure drops experience 4 and 7 orders of magnitude reduction during shear displacement, respectively, and (iii) the critical Reynolds number varies from 0.001 to 25 and experiences 4 orders of magnitude enlargement by increasing shear displacement from 0 to 20 mm. These findings may prove useful in proper understanding of fluid flow through rock fractures, or inclusions in computational studies of large-scale nonlinear flow in fractured rocks.

1. Introduction

The hydraulic, mechanical, and coupled hydromechanical behavior of rock masses are of considerable interest in many natural phenomena in hydrogeology and geophysics. Moreover, these behaviors are very important in engineering applications such as reservoir exploitation for water supply, petroleum, geothermal, and heat storages. Therefore, it is becoming essential to be able to characterize the physical processes governing hydraulic and mechanical interactions of individual fractures that could be the fundamental elements to understand the coupled hydromechanical behavior of rock masses.

The hydraulic behavior of rock fractures is significantly dependent upon the geometry of void space where the change in the geometry or aperture has obvious implications for fluid flow [*Cook*, 1992; *Isakov et al.*, 2001; *O'Brien et al.*, 2003; *Ogilvie et al.*, 2006; *Pyrak-Nolte et al.*, 1988; *Tsang and Witherspoon*, 1981]. When shearing of a rough fracture occurs, the opposed contacting asperities slide over each other that cause surface damages [*Jing et al.*, 1992; *Pereira and de Freitas*, 1993] and increasing in the aperture or dilatancy [*Barton et al.*, 1985; *Holland et al.*, 2011]. Consequently, the fracture geometry and its attributes such as contact ratio, dilation, relative roughness, and matedness experience rigorous disturbances during shear processes [*Sharifzadeh et al.*, 2006]. Therefore, rigorous disturbances in the hydraulic behavior of fracture will be anticipated during shear [*Auradou et al.*, 2005, 2006; *Boulon et al.*, 1993; *Esaki et al.*, 1991, 1999; *Gentier et al.*, 2000; *Giger et al.*, 2011; *Hans and Boulon*, 2003; *Koyama et al.*, 2006; *Li et al.*, 2008; *Matsuki et al.*, 2010; *Olsson*, 1992; *Olsson and Barton*, 2001; *Olsson and Brown*, 1993; *Sharifzadeh*, 2005; *Xiong et al.*, 2011; *Yeo et al.*, 1998] that is the main contribution of this paper.

The general description of Newtonian fluid motion in a rough-walled fracture is given by the Navier-Stokes (NS) equations composed of a set of coupled nonlinear partial derivatives of varying orders [*Brush and Thomson*, 2003; *Javadi et al.*, 2010; *Zimmerman and Bodvarsson*, 1996)]. Unfortunately, the existence and uniqueness of closed form solution of the full NS equations in three dimensions is not proven yet. On the other hand, the simplified forms of the NS equations such as linear Stokes equation [*Brown et al.*, 1995; *Mourzenko et al.*, 1995] and the Reynolds lubrication equation [*Brown*, 1987; *Ge*, 1997; *Nicholl et al.*, 1999; *Oron and Berkowitz*, 1998; *Renshaw*, 1995; *Talon et al.*, 2010] are just valid for laminar flow, diminishing the inertia effects, through fractures with especial geometrical conditions that are rarely encountered for natural fractures subjected to in situ stress.

The linearity of Darcian flow comes from the diminishing the inertia effects (i.e., kinetic energy) that can only be anticipated for low flow rates. By increasing the flux, inertial terms cannot be neglected with regard to viscous forces and the pressure drop increases more than the proportional increases in the flux that is known as the nonlinear fluid flow [*Cooke*, 1973; *Elsworth and Doe*, 1986; *Holditch and Morse*, 1976; *Jung*, 1989; *Kohl et al*., 1997; *Wen et al*., 2006; *Yeo and Ge*, 2001]. Flow regimes and nonlinear behavior of fluid flow through fractures have been investigated empirically [*Elsworth and Goodman*, 1986; *Lomize*, 1951; *Louis*, 1969], experimentally [*Cherubini et al*., 2012; *Cornwell and Murphy*, 1985; *Davies and White*, 1928; *Huitt*, 1956; *Ji et al*., 2008; *Konzu and Kueper*, 2004; *Nowamooz et al*., 2009; *Parrish*, 1963; *Qian et al*., 2005, 2011; *Quinn et al*., 2011; *Ranjith and Darlington*, 2007; *Ranjith and Viete*, 2011; *Zimmerman et al*., 2004], and numerically [*Bués et al*., 2004; *Javadi et al*., 2010; *Kolditz*, 2001; *Skjetne et al*., 1999]. These studies propose that nonlinearity in flow through fractures becomes increasingly significant with increasing the Reynolds number. The "critical" Reynolds number characterizes the onset of flow transition to nonlinear. However, a wide range of critical Reynolds numbers from 1 to 2300 has been suggested for fractures [*Cornwell and Murphy*, 1985; *Davies and White*, 1928; *Huitt*, 1956; *Ji et al*., 2008; *Konzu and Kueper*, 2004; *Louis*, 1969; *Parrish*, 1963; *Ranjith and Viete*, 2011; *Skjetne et al*., 1999; *Zimmerman et al*., 2004]. The possible explanations of the discrepancy between these arguments can be addressed by the mismatched definitions of the flow regime transition, nonunique criteria of the flow nonlinearity, and a sufficiently wide range of the geometrical characteristics of the fracture and flow conditions that covered the data and correlations of these studies. For instance, by increasing the fracture roughness, the critical Reynolds number will rapidly decrease [*Javadi et al*., 2010; *Konzu and Kueper*, 2004; *Parrish*, 1963; *Ranjith and Darlington*, 2007; *Zimmerman et al*., 2004]. However, it is questionable whether these critical Reynolds numbers are valid for natural rough-walled fractures that are subjected to field stress or mechanical displacements. Although the above researches represent a significant step forward in deepening our qualitative understanding of the nonlinear fluid flow and hydromechanical behavior of rough rock fractures, few efforts have been implemented on the influence of the shear processes on the critical Reynolds numbers.

The main purpose of this paper is to experimentally elucidate the role of shearing on the variation of critical Reynolds number and nonlinearity of fluid flow through rough-walled rock fractures. To reach this goal, first a criterion for flow nonlinearity so-called "CFN model" was developed to quantify the onset of nonlinear flow by comprehensive combination of Reynolds number and Forchheimer's law. A series of hydromechanical laboratory investigations were performed on different initially closely mated rock fractures undergoing shear to evaluate effects of mechanical displacements on the hydraulic behavior. At each shear displacement, several high-precision water flow tests were carried out with different hydraulic gradients and critical Reynolds number was calculated based on the CFN model. Finally, the variation of critical Reynolds number with shearing was analyzed using mechanical behavior of fractures recorded during shear-flow laboratory investigations.

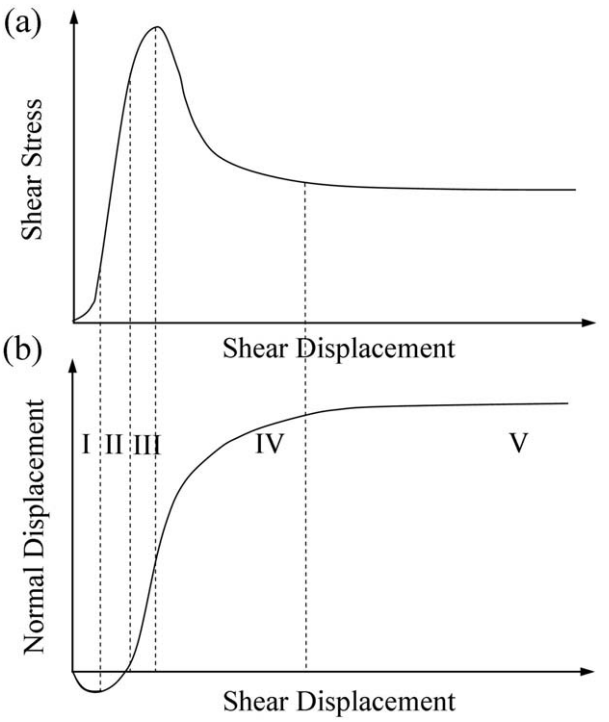

Figure 1. Typical behavior of fresh rock fractures under laboratory direct shear test condition: (a) shear stress and (b) normal displacement.

2. Theory and Background

2.1. Fracture Shear Behavior

The typical shear behavior of a rough-walled rock fracture under direct shear laboratory test condition and a constant normal stress is ideally illustrated in Figure 1. As shown in Figure 1a, the

shear behavior presents an unstable mode of failure where the shear strength shows a remarkable drop from the peak strength at small displacements to lower residual one at large displacement. In fact, the shear stress increases rapidly until the peak strength is reached. As the displacement continues, the shear stress will fall to residual value that will then remain constant, even for large shear displacements. Due to the roughness of the fracture surfaces, the shear displacement is accompanied with normal displacement, dilation, as shown in Figure 1b. The dilatancy of rough-walled fractures shows a nonlinear manner. The rate of dilation is greatest at small shear displacements, decreases after the peak shear stress, and approaches a constant value during the residual region when shear stress also approaches a constant value.

The shear characteristic of rock fractures influenced by a large extent on several phenomena and many effective factors including wall strength and weathering state [*Barton*, 1973, 1976; *Bandis et al*., 1983], boundary conditions and normal stresses [*Haberfield and Johnston*, 1994; *Haberfield and Seidel*, 1999; *Haque*, 1999; *Jiang et al*., 2004; *Leichnitz*, 1985; *Pereira and de Freitas*, 1993; *Saeb and Amadei*, 1992; *Seidel and Haberfield*, 2002; *Sun et al*., 1985], time [*Dieterich*, 1972; *Ruina*, 1983], deformation history [*Babanouri et al*., 2011; *Belem et al*., 2007; *Boulon et al*., 2002; *Chern et al*., 2012; *Dowding et al*., 1991; *Huang et al*., 1993], fracture geometry and roughness [*Archambault et al*., 1997; *Barton*, 1973, 1976; *Barton et al*., 1985; *Gentier et al*., 2000; *Goodman*, 1969; *Grasselli et al*., 2002; *Huang et al*., 2002; *Karami and Stead*, 2008; *Kwafniewski and Wang*, 1997; *Lopez et al*., 2003; *Park and Song*, 2009; *Zhang et al*., 2006; *Zhao*, 1997], shear direction [*Jing et al*., 1992, 1994], and scale [*Bandis et al*.,1981; *Barton and Bandis*, 1980; *Barton et al*., 1985]. From these, fracture geometry and surface roughness play a key role in the shear characteristic of rock fractures. The unstable mode of shear stress displacement (Figure 1) is caused by processes arising from surface mismatch, surface disturbances and asperity damages. The asperities on fracture surface can be divided into two categories including primary asperities and high-order asperities. The primary asperities have the largest wavelengths compared with the dimension of the specimen and the high order or secondary asperities are much smaller in size. Based on the above studies, the shear stress-displacement behavior and corresponding dilatancy of initially matched and fresh (without previous shear deformation) rough-walled fractures can be divided into five phases:

1. *Initial closure:* As shear stress is applied, two fracture surfaces are settled and interlocked. Therefore, the fracture experiences negative dilation or closure. In this step, the stiffness and contact area are increased without remarkable damages in asperities [*Moradian et al*., 2010].

2. *Linear prepeak*: This phase shows nearly linear or elastic deformations. The slope of the shear stress-displacement curve remains constant and loading does not produce irreversible damages in asperities. Dilation starts to increase along this phase due to the sliding of the high-order asperities.

3. *Nonlinear prepeak:* This phase starts with transition from linear to irreversible nonlinear behavior at the yield point with corresponding yield shear stress. By increasing shear displacement, the high-order asperities in the actual contact area are gradually sheared off or broken away, therefore, providing resistance to the shear displacement. Dilation increases along this phase because of the sliding and damaging of the high-order asperities. This period is ended by peak shear stress where dilatancy shows its maximum rate.

4. *Postpeak:* The shear stress-displacement curve shows a progressive softening behavior. During this phase, most of the high-order asperities are broken and primary asperities, in contact, start to damage (depending on the amount of normal stress). After peak shear stress, the resistance from the high-order asperities becomes negligible because they are mostly sheared off. The contact area and rate of dilation decrease after the peak shear stress due to the overriding of the asperities on the opposing rough surfaces.

5. *Residual:* The rate of dilation decreases dramatically and approaches a constant value during this phase. Shear stress also falls to a constant value corresponds to the residual friction resistance that depends on the rock type and damaged surface morphology. Asperities degradation is continued, but in a lower intensity than postpeak phase.

All these processes associate with rigorous changes in fracture geometry that has obvious disturbances on hydraulic behavior. Therefore, proper solution for hydromechanical problems will require fundamental understanding of the surface damages and externally measured displacements that sustain during shear sliding.

2.2. Fluid Flow Through Fractures

The general description of fluid flow in a single fracture is given by the NS equations which express momentum and mass conservation over the fracture void space. Considering the steady laminar flow of a

Newtonian fluid with constant density and viscosity through a fracture with impermeable walls, the NS equations may be written in vector form as [*Brush and Thomson*, 2003]

$$\rho(\boldsymbol{u}.\nabla)\boldsymbol{u}=\mu\nabla^2\boldsymbol{u}-\nabla p, \tag{1}$$

where $\boldsymbol{u}=(\boldsymbol{u_x}, \boldsymbol{u_y}, \boldsymbol{u_z})$ is the flow velocity vector, ρ is the fluid density, μ is the fluid dynamic viscosity, and p is the hydrodynamic pressure. Equation (1) is composed of a set of coupled nonlinear partial derivatives of varying orders. In order to have a closed system of equations, they must be supplemented by the continuity equation, which represents conservation of mass. For an incompressible fluid, conservation of mass is equivalent to conservation of volume, and the equation takes the form [*Zimmerman and Bodvarsson*, 1996],

$$\nabla.\boldsymbol{u}=0. \tag{2}$$

The complexity of these equations, combined with the complicated geometry of rock fracture, renders them difficult to solve. Therefore, further simplifications are usually adopted to overcome the difficulties of working with the NS equations. By assuming that inertial forces in the fluid are negligible compared with the viscous and pressure forces, the NS equations can be reduced to solvable forms such as linear Stokes equation. For viscous flow, linear Stokes equation, under uniform one-dimensional pressure gradient between two smooth parallel plates, well known as Poiseuille flow, the total volumetric flow rate through the fracture, Q, is given by

$$Q=-\frac{wa^3}{12\mu}\nabla p=-\frac{kA_f}{\mu}\nabla p, \tag{3}$$

where w is the fracture width (perpendicular to the pressure gradient), a is the aperture of the idealized parallel smooth fracture, k is the fracture permeability, and A_f is the cross-section area. This equation is commonly referred to as "cubic law" [*Witherspoon et al*., 1980], which predicts that the flow rate is proportional to the cube of aperture (for idealized fracture with parallel and smooth surfaces). The linear relationship between the flow rate and the pressure gradient comes from the diminishing the inertia effects (i.e., kinetic energy) that can only be anticipated for low flow rates. By increasing the flux, the pressure drop increases more than the proportional increases in the flux that is known as the nonlinear flow [*Elsworth and Doe*, 1986; *Jung*, 1989; *Wen et al*., 2006; *Yeo and Ge*, 2001]. The most classical approach for the mathematical description of the nonlinear flow through fractures is the use of the Forchheimer's law as [*Bear*, 1972]

$$-\nabla p=\frac{\mu}{k}\boldsymbol{u}_x+\rho\bar{\beta}\boldsymbol{u}_x|\boldsymbol{u}_x|, \tag{4a}$$

$$-\nabla p=AQ+BQ^2, \tag{4b}$$

where $\bar{\beta}$ is called non-Darcy coefficient or inertial resistance with dimension of L^{-1}, A and B are coefficients that describe energy losses due to viscous and inertial dissipation mechanisms, respectively [*Moutsopoulos*, 2009]. It should be noted that, the coefficient of A is equal to $\frac{\mu}{T}$, where T is the transmissivity. It is generally accepted that the Forchheimer's law adequately describes the nonlinear fluid flow through rough-walled rock fractures, especially for strong inertia regime [*Al-Yaarubi et al*., 2005; *Cherubini et al*., 2012; *Cooke*, 1973; *Holditch and Morse*, 1976; *Ji et al*., 2008; *Kohl et al*., 1997; *Konzu and Kueper*, 2004; *Moutsopoulos*, 2009; *Nowamooz et al*., 2009; *Qian et al*., 2011; *Quinn et al*., 2011; *Ranjith and Darlington*, 2007; *Ranjith and Viete*, 2011; *Skjetne et al*., 1999; *Zimmerman et al*., 2004]. For practical purposes, it can be demonstrated that the Forchheimer's law can probably be applied over the entire range of flow rates where it effectively reduces to Darcy's law at low flow rates. Therefore, the nonlinear analysis of fluid flow through fractures and development of criterion for flow nonlinearity in this paper were implemented based on the Forchheimer's law.

Generally, the onset of flow transition to nonlinear can be characterized by two different dimensionless numbers known as Forchheimer number and Reynolds number. The Forchheimer number is defined as the ratio of nonlinear to linear pressure losses or the ratio of the quadratic coefficient to the linear

coefficient in the Forchheimer's law. Based on the equation (4b), the Forchheimer number, F_O, can be formulated as,

$$F_O = \frac{BQ^2}{AQ} = \frac{BQ}{A}. \tag{5}$$

The Reynolds number gives a measure to compare the ratio of inertial forces to viscous forces and consequently quantifies the relative importance of these two types of forces for given flow conditions. For flow through fractures, the Reynolds number, *Re*, is defined as [*Zimmerman et al*., 2004]

$$Re = \frac{\rho \bar{v} D}{\mu} = \frac{\rho Q}{\mu w}, \tag{6}$$

where $\bar{v}$ is the average velocity and D is the characteristic dimension of the flow system that equals to mean aperture of fracture. The "critical" Reynolds number characterizes the onset of flow transition to nonlinear and can be defined as the point at which the nonlinear pressure drop contributes α percentage of the overall pressure drop. Considering the Forchheimer's law, the role of nonlinear pressure drop (or pressure gradient) reaches to α percentage of the overall pressure drop where,

$$\alpha = \frac{BQ^2}{AQ + BQ^2} = \frac{F_O}{1 + F_O}. \tag{7}$$

The criterion for flow nonlinearity so-called "CFN model" that defines the critical Reynolds number, Re_c, can be obtained by simplifying equation (7) and introducing into equation (6) as,

$$Re_c = \frac{A\rho\alpha}{B\mu w(1-\alpha)}. \tag{8}$$

This equation shows a simple measure to quantify the critical Reynolds number for onset of nonlinear flow through rough-walled fractures. It should be noted that the Forchheimer number is implicitly involved in the CFN model. In fact, the term $\frac{\alpha}{(1-\alpha)}$ in this equation is the Forchheimer number that can be inferred by simplifying equation (7). Moreover, the critical Reynolds number in equation (8) can be defined as the ratio of Forchheimer number to dimensionless Forchheimer coefficient, β, introduced by *Zimmerman et al*. [2004] in the form of $Re_c = \frac{F_O}{\beta}$.

In recent studies, the critical condition for onset of flow nonlinearity has been defined as the point at which the nonlinear pressure drop contributes, say, 10% of the overall pressure drop [*Zeng and Grigg*, 2006; *Zimmerman et al*., 2004], that is equal to $\alpha = 0.1$ or $F_O = 0.11$. Considering this condition, the critical Reynolds number for nonlinear fluid flow through rough-walled fractures will be suggested as,

$$Re_c = \frac{A\rho}{9B\mu w}. \tag{9}$$

3. Experimental Setup

3.1. Specimen Preparation

Granite specimens of 180 mm in length, 100 mm in width, and 80 mm in height were used for hydromechanical experiments. Specimens were provided from intact hard granite (unit weight 2.61 g/cm^3, porosity 0.37%, uniaxial compressive strength 172 MPa). An artificial fracture was created at midheight of each intact rock specimen using a generator apparatus consists of horizontal and normal loading jacks and a steel guide box that is schematically shown in Figure 2a. To create this fracture correctly and easily, two saw-cut slits with 1 mm width and 5 mm depth are initially generated at the midheight of the intact rock specimen. The intact specimen with saw-cut slits is set in the fracture generator apparatus and a normal load about 200 kN (or about 8.5 MPa) is applied on the upper face of specimen. A pair of steel wedges are placed in

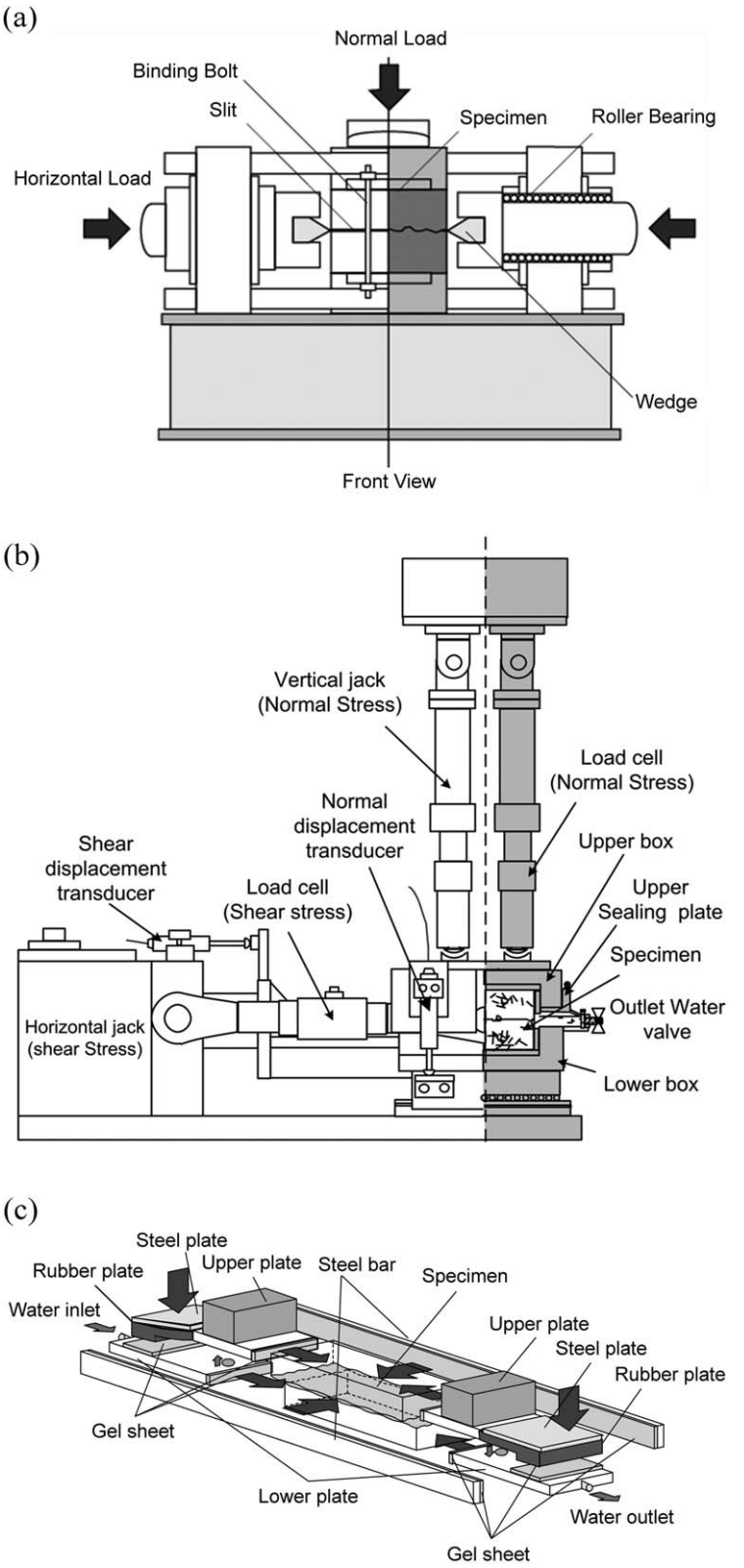

Figure 2. Schematic view of the experimental setup: (a) fracture generator apparatus, (b) shear-flow test apparatus, and (c) hydraulic sealing around specimen [after *Mitani et al*., 2005].

the saw-cut slits on the opposite faces and a constant horizontal load about 120 kN is applied through this steel wedges. Then the normal load is gradually decreased until the wedges penetrate into the specimen, and the split is extended by tensile failure. During the fracture generation, horizontal load is kept constant. Thus, specimen is fractured smoothly under controlled conditions without causing violent vibrations and crashing.

3.2. Shear-Flow Test Apparatus

Figure 2b shows a schematic view of the apparatus used for investigating the coupled shear-flow behavior of rough-walled rock fractures. This apparatus consists of three main unites: mechanical testing unit, hydraulic testing unit, and a control and data acquisition system. The shear and normal stresses, shear and normal displacements, and water flow rate can be measured precisely and continuously using this apparatus. The advantage of this apparatus is its simplicity in operation and measurement, easy control of combination of normal and shear stresses and possible measurement of large shear deformation in case of a test of preexisted fracture (for more information, please see the *Mitani et al.* [2005] and *Sharifzadeh* [2005]).

3.2.1. Mechanical Testing Unit

The mechanical testing unit consists of normal and shear loading unit. Direct shear loading unit consists of a shear box with upper and lower parts. The fracture is set in the shear box and sheared by moving the lower part of shear box. The upper part of the shear box is connected by a pair of tie rods to a horizontal jack which allows the upper part to move vertically and rotate, but the horizontal movement is restricted. Two tensile-compressive load cells, used for measuring shear load, are set in the tie rods to both horizontal sides of the shear box. Shear loads can be arbitrarily applied on the fracture by a servo-control system. Shear displacement is measured by a strain transducer with resolution of 10^{-3} strain/mm and precision of 10^{-2} strain $\pm$ 0.1% installed between the horizontal jack and the upper shear box.

The normal loading unit has two normal tie rods with normal loading jacks and load cells to supply low to high normal stresses and control the inclination of the upper shear box. Normal and shear loads controlled independently by two separate servo systems. Normal displacements during shear of specimen are measured by four displacement transducers attached on each corner of the upper shear box. Both load and displacements in the normal and shear directions from load cells and transducers, respectively, are automatically recorded by data loggers.

3.2.2. Hydraulic Testing Unit

The hydraulic testing unit consists of fracture sealing system, inlet water supply into the fracture, discharged outlet water collection, and measurement system. This testing unit has been developed for one-dimensional flow experiments (with constant head) through rock fracture undergoing normal or shear loading. Therefore, lateral sides of the specimen must be sealed during flow tests. The perspective view of the sealing system of fracture specimen is shown in Figure 2c. A special rubber material, so-called "gel sheet" is placed on all sides of the fractured specimen to prevent water leakage during flow test.

Inlet water is supplied over the entire width of the fracture specimen. Inlet water head, or pressure, is regulated through the pressure gauge according to required for constant head hydraulic test. Before injecting water into the fracture, the air bubbles in inlet water tank are removed by using vacuum pump. During the test, water pressure is recorded by data logger within defined time intervals of 5 s. Water discharge from outlet is collected over the entire width of fracture. Flow rates are measured using an electric balance with precision of 0.01 g. All the measured data from different pressure transducer (DPT) or electric balance are recorded with a data logger system (every 5 s) and saved on personal computer.

3.3. Experimental Procedure

The coupled shear-flow tests were conducted on three different fracture specimens CI, CII, and CIII under constant normal stresses of 1, 3, and 5 MPa, respectively. Direct shear tests were performed based on controlling shear displacement. Shear displacement was applied with a rate of 0.1 mm/min up to the maximum displacement of 20 mm. Normal displacement and shear stress were continuously recorded with 0.05 mm of shear displacement increments. Constant head hydraulic tests were performed stepwise with 0.5, 1, and 5 mm of shear displacement increments depending on the sensitivity and importance of shear phases. Steady-state fluid flow rate throughout the joint was measured at each shearing step by keeping the normal stress and shear displacement constant. Various hydraulic tests were performed with different pressure drops between fracture inlet and outlet ranging from 3.6 to 30 kPa. For CIII specimen, the upper limit of

pressure drop extended to 54 kPa for the first 2 mm shear displacements due to the higher normal stress applied on the specimen. Each flow test starts with regulation of inlet water pressure. Then, the water inlet valve is opened to flow water through the fracture. Flow test is continually performed for a proper time until reaching a constant flow rate to achieve steady-state condition.

4. Results

4.1. Mechanical Behavior

Three different fracture specimens CI, CII, and CIII under constant normal stresses of 1, 3, and 5 MPa, respectively, were used for coupled shear-flow tests. Variation of shear stress with respect to shear displacement under constant normal stress for all cases is shown in Figure 3. For all the cases, shear stress increases quickly from zero to peak stress highly depending on the applied normal stress. The peak shear stress for CI, CII, and CIII are 0.882, 5.724, and 8.386 MPa, respectively. By increasing normal stress, the shear stress reaches the peak value at smaller shear displacement where the peak shear stress observes in shear displacement of 2.98, 2.046, and 1.968 mm for CI, CII, and CIII, respectively. This means that shear stiffness increases with increasing the applied normal stress. After peak, the shear stress falls suddenly for CII and CIII and decreases gradually to reach the residual. During residual region, shear displacements are continued with stick-slip phenomena. But for CI, shear stress follows by a gradual decrease after peak. Moreover, difference between peak and residual shear stresses increases with increasing the applied normal stress.

Figure 4 shows the shear displacement versus normal displacement of fractures during direct shear. Normal displacement was calculated as arithmetic mean of the values recorded by four displacement transducers. As shown in Figure 4, fracture normal displacement during shear shows a nonlinear descending-ascending behavior. As shear stress is applied, fractures experience negative normal displacement or closure due to the surfaces interlocking. In initial closure region, fracture normal displacement continues to decrease until reaches its minimum. The minimum normal displacements for CI, CII, and CIII are −0.0175, −0.014, and −0.017 mm, respectively. The corresponding shear displacements of minimum normal displacement for CI, CII, and CIII are 1.207, 0.914, and 0.856 mm, respectively, decreasing with increasing the applied normal stress. Fracture normal displacement begins to increase with starting linear prepeak phase and reaches the zero value at shear displacement of 1.43, 1.73, and 1.353 mm for CI, CII, and CIII, respectively.

As shown in Figure 4, the normal displacements corresponding to peak shear stress for CI, CII, and CIII are 0.267, 0.131, and 0.104 mm, respectively, decreasing with increasing the applied normal stress. The rate of normal displacement increment reaches to maximum after peak shear stress, and then decreases steadily until approaches to a constant value. Comparison of the rate of normal displacement increment after peak shear stress shows that the highest rate occurs for CI, and the lowest is for CIII. Moreover, the fracture normal displacement corresponding to residual step decreases with increasing the applied normal stress, where the smallest and largest fracture normal displacements at shear displacement of 20 mm are observed for CIII and CI, respectively.

4.2. Nonlinear Fluid Flow

During shear processes of fractures, one-dimensional steady-state flow tests were performed stepwise with 0.5, 1, and 5 mm of shear displacement increments. At each shearing step, several hydraulic tests were

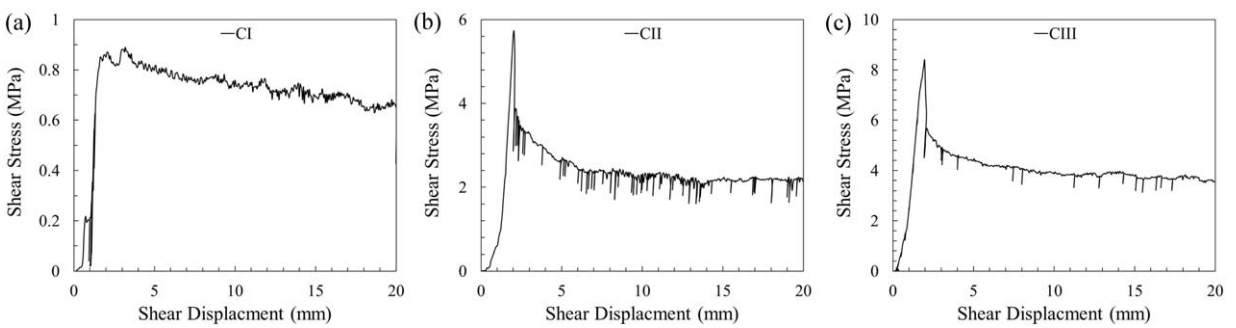

Figure 3. Shear stress versus shear displacement of fracture specimens during direct shear under constant normal stress: (a) CI, (b) CII, and (c) CIII (note that the vertical axes are not in the same scale).

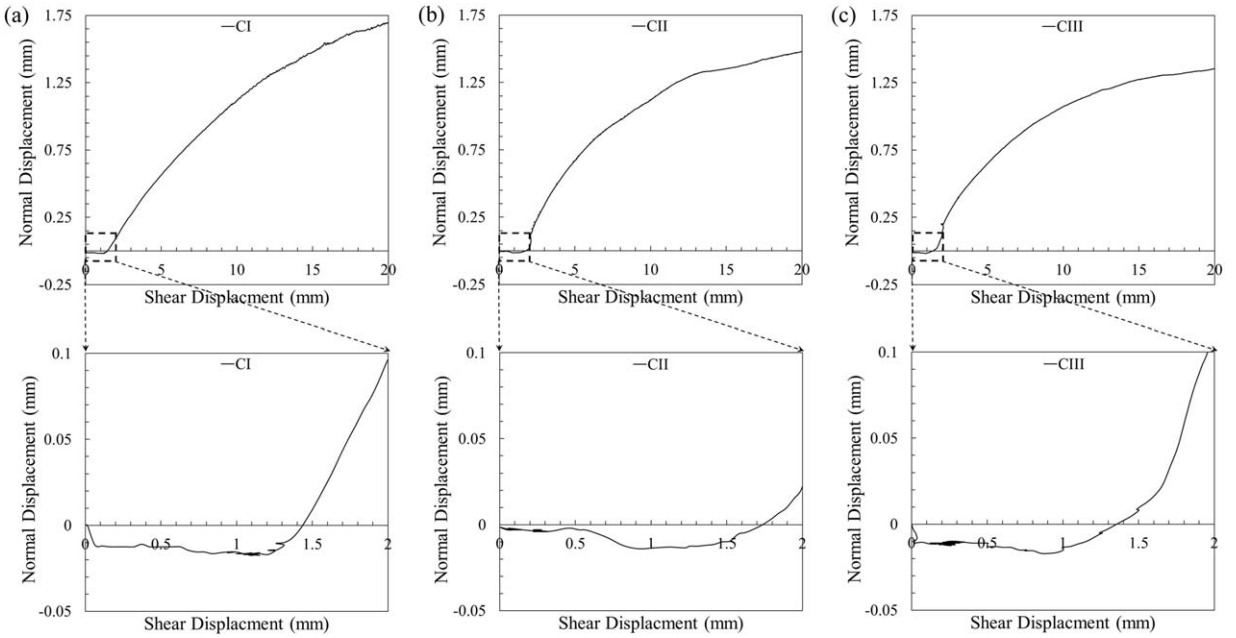

Figure 4. Normal displacement versus shear displacement of fractures during shear under constant normal stress: (a) CI, (b) CII, and (c) CIII.

performed with different pressure gradients between fracture inlet and outlet. Results of these hydraulic tests were used for investigating the nonlinear flow. At each shearing step, quadratic polynomial regression in the form of equation (4b) was fitted to the result of hydraulic tests and the coefficients *A* and *B* were calculated. To reach a polynomial in the form of equation (4b), the intercept was set to be zero for quadratic polynomial regression. The quadratic polynomial regression was properly fitted to the experimental results. An exception to this was the data measured for CIII at zero shear displacement. This data was found to be erratic in scattering possibly because of measurement errors and therefore was not considered in the analysis.

The results of quadratic polynomial regression provide a good accuracy, where the residual squared R^2 is greatest 0.99 for all shearing steps in the cases of CI and CIII. For CII, the quadratic polynomial regression provides R^2 about 0.921, 0.973, and 0.957 for shear displacements of 2, 3, and 5 mm, respectively. Other results for CIII give R^2 greatest 0.99. Figure 5 shows the quadratic polynomial regression for hydraulic tests, for instance, on CII in 4 mm shear displacement. The fitted quadratic polynomial expression in the form of the Forchheimer's law consists of a linear term (AQ) and a nonlinear term (BQ^2) describing viscous and inertial pressure drops, respectively. The role of linear and nonlinear terms in overall pressure drop (or pressure gradient) is shown in Figure 5. At low flow rates, both the Forchheimer's law and linear term

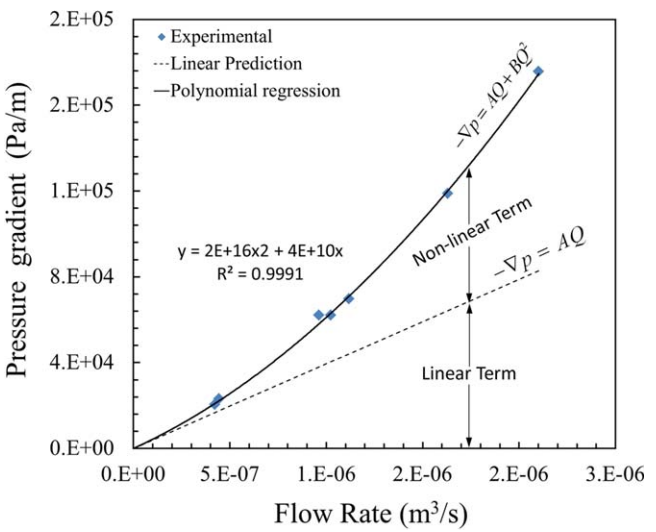

Figure 5. The role of linear and nonlinear terms in overall pressure drop and quadratic polynomial regression for hydraulic tests (Results from CII in 4 mm shear displacement).

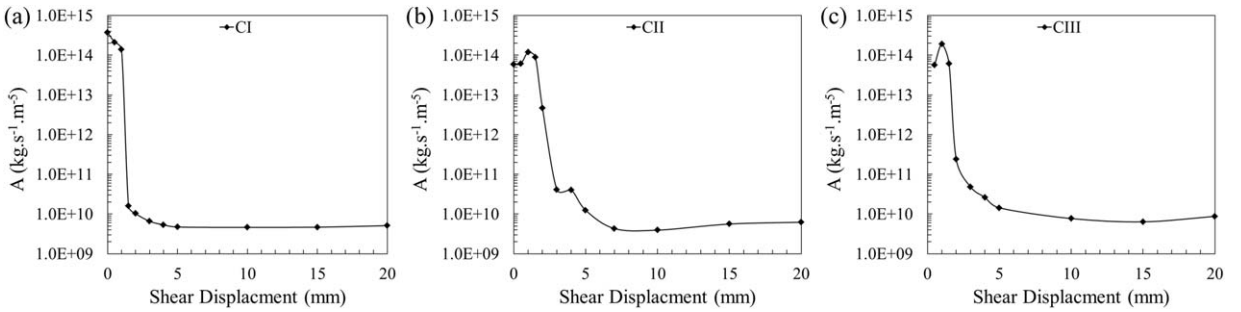

Figure 6. Variation of the coefficient A during shear: (a) CI, (b) CII, and (c) CIII.

propose close pressure drops. Since the Forchheimer's law successfully reduces to Darcy's law at low flow rates, it can be applied over the entire range of flow rates. By increasing flow rate or Reynolds number, deviation from the linearity in flow through fracture becomes more evident and inertial pressure drop cannot be neglected with regard to viscous pressure drop.

At each shearing step, the coefficients *A* and *B* were calculated using quadratic polynomial regression. Figure 6 shows variation of the coefficient *A* during shear. As shown in Figure 6, the coefficient *A* experiences about 4 orders of magnitude reduction during shear. For CI, the coefficient *A* shows a descending variation during shear. As shown in Figure 6a, the coefficient *A* falls suddenly in shear displacement between 1 and 1.5 mm, where it decreases about 4 orders of magnitude. After shear displacement of 1.5 mm, the coefficient *A* decreases gradually to attain a somewhat constant value for shear displacements exceeding 5 mm. For CII and CIII, the coefficient *A* shows an ascending-descending variation during shear. The coefficient *A* for both CII and CIII reaches its maximum at shear displacement of about 1 mm and falls suddenly after 1.5 mm shear displacement. After shear displacement of about 3 mm, the coefficient *A* decreases gradually to attain a somewhat constant value for shear displacements exceeding about 7 and 10 mm for CII and CIII, respectively.

Variation of coefficient *B* during shear processes is shown in Figure 7. The coefficient *B* shows a descending variation for CI and CIII, and an ascending-descending variation for CII. The coefficient *B* shows an abrupt reduction during the prepeak regions (for shear displacements between 1 and 2 mm). The reduction rate of the coefficient *B* decreases after shear displacement of about 3 mm. From Figures 6 and 7, it can be found that the variation pattern of coefficients *A* and *B* are very similar. However, the reduction rate of the coefficient *B* is much higher than *A*. Figure 7 shows that the coefficient *B* experiences about 7 orders of magnitude reduction during shear.

At each shearing step, the critical Reynolds number was calculated using CFN model by considering $\alpha = 0.1$. Variation of critical Reynolds number during shear is shown in Figure 8. As shown in Figure 8, the critical Reynolds number experiences about 4 orders of magnitude enlarging by increasing shear displacement from 0 to 20 mm. For all the cases and shear displacements lower than 1 mm, the critical Reynolds number is lower than 0.04. The critical Reynolds number shows an ascending variation for CI and CIII. For CI, the critical Reynolds number shows an enormous increase for shear displacements between 1 and 1.5 mm and

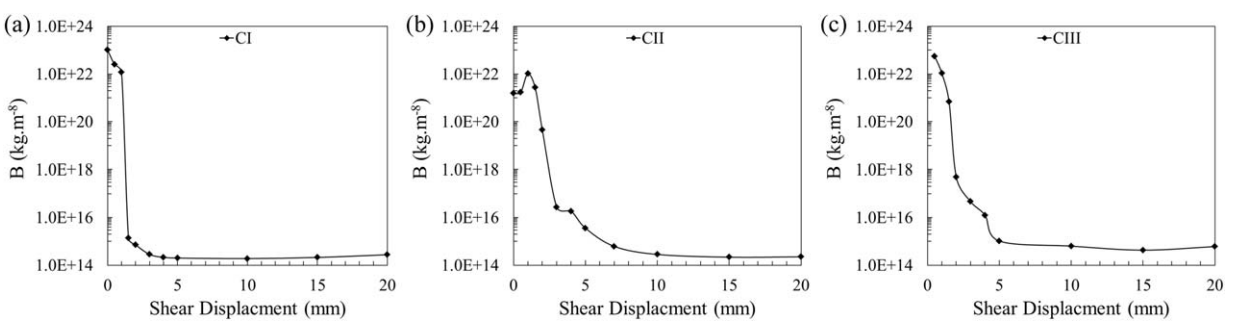

Figure 7. Variation of the coefficient B during shear: (a) CI, (b) CII, and (c) CIII.

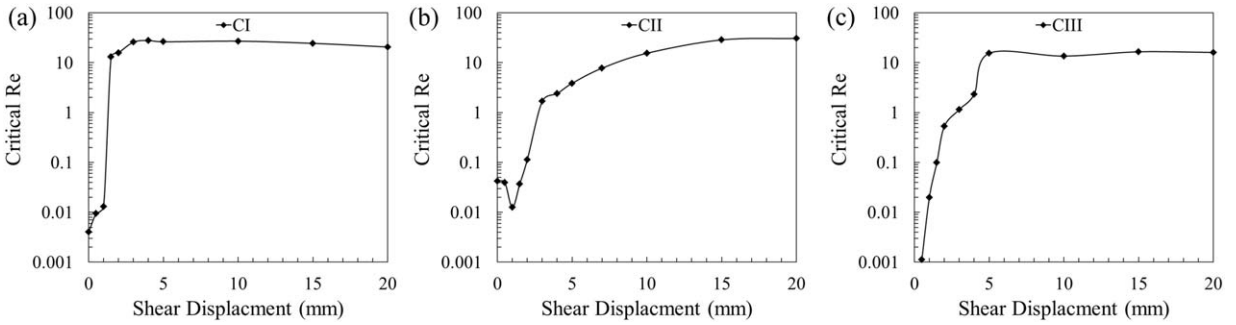

Figure 8. Critical Reynolds number during shear: (a) CI, (b) CII, and (c) CIII (the critical Reynolds number was calculated using NCF model by considering $\alpha = 0.1$).

attains a somewhat constant value in the range of 25 for shear displacements exceeding 3 mm. For CIII, the critical Reynolds number increases almost consistently by increasing shear displacement and reaches a somewhat constant value in the range of 15 for shear displacements exceeding 5 mm. As shown in Figure 8b, the critical Reynolds number shows a descending-ascending variation for CII. For this case, the critical Reynolds number falls from 0.004 to 0.001 for shear displacements from 0 to 1 mm. After shear displacement of 1 mm, the critical Reynolds number increases gradually to attain a somewhat constant value for shear displacements exceeding 15 mm (Figure 8b).

5. Discussion

It is well clear that, fracture geometry and surface roughness play a key role in the both hydraulic and mechanical characteristic of rock fractures. A typical natural fracture in rock masses consists of two rough-walled surfaces with complex morphology varies over the fracture. Therefore, regardless of the fracture size, the aperture distribution always has a strong heterogeneity due to a wide range of the aperture and a significant number of the contact points [*Tsang*, 1984; *Witherspoon et al*., 1980; *Xiong et al*., 2011]. When fluid flows through such a fracture, it not only flows around the contact areas, but also has a tendency to flow through the channels with the largest apertures [*Archambault et al*., 1997; *Brown*, 1987; *Li et al*., 2008; *Neuzil and Tracy*, 1981; *Tsang and Tsang*, 1987; *Watanabe et al*., 2008]. Since the flow occurs over a few tortuous channels, the hydraulic behavior of fracture would be controlled by the small apertures and constrictions [*Tsang and Tsang*, 1987; *Neuzil and Tracy*, 1981]. The structure of the aperture field is strongly related to the relative position of the fracture surfaces together with the statistical distribution of the asperities [*Auradou*, 2009]. Due to the roughness of the fracture surfaces, the shear displacement is accompanied with two main features including dilation and lateral mismatching of surfaces [*Esaki et al*., 1999]. Both of these features remarkably change the fracture geometry and its attributes such as contact ratio, relative roughness, and spatial distribution of aperture [*Sharifzadeh et al*., 2006]. Due to the changes in the shape of the aperture distribution, contact area, and degree of mismatching governing by shear process, significant variations are expected in the coefficients *A* and *B* and the critical Reynolds number as a result.

Nonlinearity of fluid flow may occur as a result of inertial losses arising from entrance and exit losses, changes in flow velocity or direction along the flow path, and localized eddy formation. Such inertial losses are generally proportional to the square of the fluid velocity [*Schrauf and Evans*, 1986] and form the repercussion of the coefficient *B*. Rapid changes in the aperture along the flow path will necessitate prompt variations in the inplane velocity, in order to maintain conservation of mass that causes acceleration and deceleration of the flow. These repeated acceleration and deceleration sequences cause a departure from a linear relationship between pressure drop and flow rate, even if the flow remains laminar [*Cornwell and Murphy*, 1985]. The magnitude of the effect of tortuosity in depressing fluid flow rate varies with the shape of the aperture distribution [*Tsang*, 1984]. Shear displacement reduces the degree of matedness between the two fracture surfaces and, as a result, the magnitudes of the components of an aperture with low frequencies (large wavelengths) increase relative to those with high frequencies, particularly for small fractures. Thus, the probability of the connectivity of large apertures greatly increases with shear displacement and, accordingly, channels may be easily created in sheared fractures [*Matsuki et al*., 2006]. On the other hand,

by increasing shear displacement, the shear induced new contact areas decrease slowly and the number of contact spots becomes much smaller and focused at a much fewer locations of larger areas of contact [*Koyama et al*., 2009]. The localization of water flow in a sheared fracture thus occurs due to the fact that a smaller number of channels and ridges with a greater area are formed as the shear displacement increases [*Matsuki et al*., 2005]. Therefore, when the fracture walls have undergone a shear displacement, high aperture channels with reduced hydraulic resistance (or coefficients *A* and *B*) develop in the fracture plane.

Since in initial closure phase two fracture surfaces are settled and interlocked, the fracture experiences closure with increasing contact area. These effects reduce the open space through which flow takes place and thereby yields significant decrease in fracture conductivity or increase in the coefficients *A* and *B*. As shown in Figure 6, the coefficient *A* shows an ascending behavior for CII and CIII in initial closure phase that confirms this physical process. However, the coefficient *A* shows a descending behavior for CI in initial closure phase. This inconsistent result possibly comes from the flow test procedure performed stepwise. Since the hydraulic tests were performed stepwise with 0.5 m shear displacement increments, the actual hydraulic behavior of fracture between consecutive shear displacement steps will be unexplored, especially when much variation of normal displacement occurs between consecutive steps. However, it is anticipated that the coefficient *A* increases in initial closure phase. Such increase is also anticipated for coefficient *B* variation in this phase. The ascending variation of coefficient *B* for CII in initial closure region justifies this postulation. But the coefficient *B* shows a descending behavior for CI in initial closure phase that possibly comes from the stepwise flow test procedure.

After linear prepeak phase, the shear processes attend by fracture dilation and damages in high-order asperities that lead increase in aperture and decrease in relative roughness and contact area. All these events associate with less deviation from the idealized flow between parallel plates, decreasing abrupt changes in the aperture along the flow path, decreasing the flow tortuosity, and less fluid velocity disturbances and eddying. These physical presences attain cause less pressure drops and thus significant reduction in flow resistance or decrease in the coefficients *A* and *B*. The intensity of the above geometrical events is much at nonlinear prepeak phase, decreasing with increasing shear displacement to reaches somewhat negligible in residual region. As shown in Figures 6 and 7, immediately after linear prepeak phase, both the coefficients *A* and *B* show an abrupt reduction. After nonlinear prepeak phase, both the coefficients *A* and *B* decrease gradually to attain a somewhat constant value in residual region. Moreover, the variation pattern of coefficients *A* and *B* are very similar but the reduction rate of the coefficient *B* is much higher than *A*. The coefficients *A* and *B* experience about 7 and 4 orders of magnitude reduction, respectively, during shear. From CFN model, it can be found that the critical Reynolds number is proportional to the ratio of *A* to *B*. Since the coefficient *B* experiences considerably much reduction than *A*, the critical Reynolds number embraces enormous enlargement during the shear processes.

The laminar flow through rock fracture is usually assumed a linear relationship between the flux and the pressure gradient that comes from the diminishing the inertia effects. Clearly, at sufficiently high flow rates, this relationship becomes nonlinear. It should be noted that deviations from linear relationship between flow rate and pressure drop are often attributed, perhaps erroneously, to turbulence. Although the intense flow nonlinearity may imply the turbulency on flow, the term "nonlinearity" of flow is only used in this paper for describing the deviations from linear relationship between flow rate and pressure drop and it does not mean that the flow regime is turbulent. Generally, the onset of flow transition to nonlinear can be characterized by two different dimensionless numbers known as Forchheimer number and Reynolds number. It should be noted that the Reynolds number quantifies the relative strength of inertia forces as compared to viscous forces at microscopic level. Microscopic inertial effects do not directly infer to macroscopic inertial effects, where high value of local or microscopic Reynolds number does not necessarily deduce nonlinear flow at macroscopic level. In fact, the effects of heterogeneities in the fracture geometry (spatial distribution of aperture and contact area) are not considered in the Reynolds number. Therefore, the critical Reynolds number is closely dependent to geometrical attributes of fracture (such as contact ratio, relative roughness, aperture, and matedness), and easily changes dramatically with variation of such attributes. Although the Reynolds number has been widely used for characterization of nonlinear flow through rough-walled fractures, a diversified amount of critical Reynolds numbers has been suggested for fractures that makes a confused condition for practical purposes. Therefore, in practical purposes, an intelligent attention should be considered about the role of geometrical attributes of fracture on the Reynolds number. Since Forchheimer

number accounts the structure of the medium, it may suggest a better indication of the degree of inertial effects on flow than Reynolds number [*Garrouch and Ali*, 2001; *Ruth and Ma*, 1992; *Zeng and Grigg*, 2006]. The proposed CFN model combines both the Reynolds and Forchheimer numbers and therefore, it provides a more meaningful criterion for identifying nonlinear flow through rough-walled fractures.

6. Conclusions

This paper experimentally explains the role of shearing on the variation of critical Reynolds numbers and nonlinearity of fluid flow through rough-walled rock fractures. First, a quantitative criterion, CFN model, was developed to quantify the onset of flow nonlinearity by comprehensive combination of Forchheimer's law and Reynolds number. Hydromechanical laboratory experiments were performed on different initially closely mated rock fractures undergoing shear to evaluate the effect of mechanical displacements on the flow nonlinearity and critical Reynolds number. At each shearing step, the critical Reynolds number was determined using the CFN model and quadratic polynomial regression in the form of Forchheimer's law that was fitted to the results of hydraulic tests with different pressure gradients. Finally, the variation of critical Reynolds number with shear processes was evaluated using mechanical behavior of fractures. Based on the presented results, the following conclusions were obtained:

1. The Forchheimer's law was fitted very well to experimental results of nonlinear flow through rough-walled fractures undergoing shear. The quadratic polynomial in the form of the Forchheimer's law consists of a linear term (AQ) and a nonlinear term (BQ^2) describing viscous and inertial pressure drops, respectively.

2. The Forchheimer's law successfully reduces to Darcy's law at low flow rates and it can be applied over the entire range of flow rates. By increasing flow rate, deviation from the linearity in flow through the fracture becomes more evident and inertial pressure drop cannot be neglected with regard to viscous pressure drop.

3. The linear and nonlinear pressure drops highly depend on the fracture geometry that involves sever disturbances during forward shear displacement. The coefficient A and B experience about 4 and 7 orders of magnitude reduction, respectively, during shear. The variation patterns of coefficients A and B are very similar but the reduction rate of the coefficient B is much higher than A.

4. The CFN model combines both the Reynolds and Forchheimer numbers that can provide a more meaningful criterion for identifying nonlinear flow through rough-walled fractures. From CFN model, the critical Reynolds number is proportional to the ratio of A to B mainly dependent on the fracture geometry.

5. The critical Reynolds number experiences 4 orders of magnitude enlargement by increasing shear displacement from 0 to 20 mm. For all the cases and shear displacements lower than 1 mm, the critical Reynolds number is lower than 0.04. The critical Reynolds number shows an enormous increase during prepeak phases and attains a somewhat constant value in the range of 15–25 in residual region.

It is tried in this paper to explain the role of shearing processes on the nonlinearity of fluid flow through rough-walled rock fractures. The results of this study represent the first step toward the understanding the nonlinear fluid flow through tough-walled fractures. Clearly, much research remains to be inspected to this class of problems, particularly to investigation of the physical nature of nonlinear flow and flow regimes, the role of fracture geometry on the three-dimensional flow field, variation of geometrical characteristics of rock fracture during different loading conditions, flow anisotropy in respect to shear direction, and correlations and scale dependency.

References

Al-Yaarubi, A. H., C. C. Pain, C. A. Grattoni, and R. W. Zimmerman (2005), Navier-Stokes simulations of fluid flow through a rock fracture, in *Dynamics of Fluids and Transport in Fractured Rocks*, edited by B. Faybishenko et al., AGU, Washington, D. C., doi:10.1029/162GM07.

Archambault, G., S. Gentier, J. Riss, and R. Flamand (1997), The evolution of void spaces (permeability) in relation with rock joint shear behavior, *Int. J. Rock Mech. Min. Sci.*, *3*(4), 14.e1–14.e15, doi:10.1016/S1365–1609(97)00046-4.

Auradou, H. (2009), Influence of wall roughness on the geometrical, mechanical and transport properties of single fractures, *J. Phys. D Appl. Phys.*, *42*(21), 214015, doi:10.1088/0022–3727/42/21/214015.

Auradou, H., G. Drazer, J. P. Hulin, and J. Koplik (2005), Permeability anisotropy induced by the shear displacement of rough fracture walls, *Water Resour. Res.*, *41*, W09423, doi:10.1029/2005WR003938.

Auradou, H., G. Drazer, A. Boschan, J. P. Hulin, and J. Koplik (2006), Flow channeling in a single fracture induced by shear displacement, *Geothermics*, *35*(5–6), 576–588, doi:10.1016/j.geothermics.2006.11.004.

Babanouri, N., S. Karimi Nasab, A. Baghbanan, and H. R. Mohamadi, (2011), Over-consolidation effect on shear behavior of rock joints, *Int. J. Rock Mech. Min. Sci.*, *48*(8), 1283–1291, doi:10.1016/j.ijrmms.2011.09.010.

Bandis, S., A. C. Lumsden, and N. R. Barton (1981), Experimental studies of scale effects on the Shear behaviour of rock joints, *Int. J. Rock Mech. Min. Sci.*, *18*(1), 1–21, doi:10.1016/0148-9062(81)90262-X.
Bandis, S. C., A. C. Lumsden, and N. R. Barton (1983), Fundamentals of rock joint deformation, *Int. J. Rock Mech. Min. Sci.*, *20*(6), 249–268, doi:10.1016/0148-9062(83)90595-8.
Barton, N. (1973), Review of a new shear-strength criterion for rock joints, *Eng. Geol.*, *7*(4), 287–332, doi:10.1016/0013-7952(73)90013-6.
Barton, N. (1976), The shear strength of rock and rock joints, *Int. J. Rock Mech. Min. Sci.*, *13*(9), 255–279, doi:10.1016/0148-9062(76)90003-6.
Barton, N., and S. Bandis (1980), Some effects of scale on the shear strength of joints, *Int. J. Rock Mech. Min. Sci.*, *17*, 69–73.
Barton, N., S. Bandis, and K. Bakhtar (1985), Strength, deformation and conductivity coupling of rock joints, *Int. J. Rock Mech. Min. Sci.*, *22*(3), 121–140, doi:10.1016/0148-9062(85)93227-9.
Bear, J. (1972), *Dynamics of Fluids in Porous Media*, Am. Elsevier, New York.
Belem, T., M. Souley, and F. Homand (2007), Modeling surface roughness degradation of rock joint wall during monotonic and cyclic shearing, *Acta Geotech.*, *2*(4), 227–248, doi:10.1007/s11440-007-0039-7.
Boulon, M., G. Armand, N. Hoteit, and P. Divoux (2002), Experimental investigations and modelling of shearing of calcite healed discontinuities of granodiorite under typical stresses, *Eng. Geol.*, *64*(2–3), 117–133, doi:10.1016/S0013-7952(01)00112-0.
Boulon, M. J., A. P. S. Selvadurai, H. Benjelloun, and B. Feuga (1993), Influence of rock joint degradation on hydraulic conductivity, *Int. J. Rock Mech. Min. Sci.*, *30*(7), 1311–1317, doi:10.1016/0148-9062(93)90115-T.
Brown, S. R. (1987), Fluid flow through rock joints: The effect of surface roughness, *J. Geophys. Res.*, *92*(B2), 1337–1347, doi:10.1029/JB092iB02p01337.
Brown, S. R., H. W. Stockman, and S. J. Reeves (1995), Applicability of the Reynolds equation for modeling fluid flow between rough surfaces, *Geophys. Res. Lett.*, *22*(18), 2537–2540, doi:10.1029/95GL02666.
Brush, D., and N. R. Thomson (2003), Fluid flow in synthetic rough-walled fractures: Navier–Stokes, Stokes, and local cubic law simulations, *Water Resour. Res.*, *39*(4), 1085, doi:10.1029/2002WR001346.
Bués, M., M. Panfilov, S. Crosnier, and C. Oltean (2004), Macroscale model and viscous–inertia effects for Navier–Stokes flow in a radial fracture with corrugated walls, *J. Fluid Mech.*, *504*, 41–60, doi:10.1017/S002211200400816X.
Chern, S.-G., T.-C. Cheng, and W.-Y. Chen (2012), Behavior of regular triangular joints under cyclic shearing, *J. Mar. Sci. Technol.*, *20*(5), 508–513, doi:10.6119/JMST-011-0428-1.
Cherubini, C., C. I. Giasi, and N. Pastore (2012), Bench scale laboratory tests to analyze non-linear flow in fractured media, *Hydrol. Earth Syst. Sci. Discuss.*, *9*, 5575–5609, doi:10.5194/hessd-9-5575-2012.
Cook, N. G. W. (1992), Natural joints in rock: Mechanical, hydraulic and seismic behaviour and properties under normal stress, *Int. J. Rock Mech. Min. Sci.*, *29*(3), 198–223, doi:10.1016/0148-9062(92)93656-5.
Cooke, C. E. (1973), Conductivity of fracture proppants in multiple layers, *J. Pet. Technol.*, *25*(9), 1101–1107, doi:10.2118/4117-PA.
Cornwell, D. K., and H. D. Murphy (1985), Experiments with non-Darcy flow in joints with large scale roughness, paper presented at International Symposium on Fundamentals of Rock Joints, Centek, Lulea.
Davies, S. J., and C. M. White (1928), An experimental study of the flow of water in pipes of rectangular section, *Proc. R. Soc. London, Ser. A*, *119*, 92–107, doi:10.1098/rspa.1928.0086.
Dieterich, J. H. (1972), Time-dependent friction in rocks, *J. Geophys. Res.*, *77*(20), 3690–3697, doi:10.1029/JB077i020p03690.
Dowding, C. H., A. Zubelewicz, K. M. O'Connor, and T. B. Belytschko (1991), Explicit modeling of dilation, asperity degradation and cyclic seating of rock joints, *Comput. Geotech.*, *11*(3), 209–227, doi:10.1016/0266-352X(91)90020-G.
Elsworth, D., and T. W. Doe (1986), Application of non-linear flow laws in determining rock fissure geometry from single borehole pumping tests, *Int. J. Rock Mech. Min. Sci.*, *23*(3), 245–254, doi:10.1016/0148-9062(86)90970-8.
Elsworth, D., and R. E. Goodman (1986), Characterization of rock fissure hydraulic conductivity using idealized wall roughness profiles, *Int. J. Rock Mech. Min. Sci.*, *23*(3), 233–243, doi:10.1016/0148-9062(86)90969-1.
Esaki, T., H. Hojo, T. Kimura, and N. Kameda (1991), Shear-flow coupling test on rock joints, paper presented at 7th International Congress on Rock Mechanics, 4 pp., Aachen, Germany, 16–20 Sep.
Esaki, T., S. Du, Y. Mitani, K. Ikusada, and L. Jing (1999), Development of a shear-flow test apparatus and determination of coupled properties for a single rock joint, *Int. J. Rock Mech. Min. Sci.*, *36*(5), 641–650, doi:10.1016/S0148-9062(99)00044-3.
Garrouch, A. A., and L. Ali (2001), Predicting the onset of inertial effects in sandstone rocks, *Transp. Porous Media*, *44*(3), 487–505, doi:10.1023/A:1010671012287.
Ge, S. (1997), A governing equation for fluid flow in rough fractures, *Water Resour. Res.*, *33*(1), 53–61, doi:10.1029/96WR02588.
Gentier, S., D. Hopkins, and J. Riss (2000), Role of fracture geometry in the evolution of flow paths under stress, in *Dynamic of Fluids in Fractured Rock*, edited by B. Faybishenko et al., AGU, Washington, D. C., doi:10.1029/GM122p0169.
Giger, S. B., M. B. Clennell, C. Harbers, P. Clark, M. Ricchetti, J. H. Ter Heege, B. B. T. Wassing, and B. Orlic (2011), Design, operation and validation of a new fluid-sealed direct shear apparatus capable of monitoring fault-related fluid flow to large displacements, *Int. J. Rock Mech. Min. Sci.*, *48*(7), 1160–1172, doi:10.1016/j.ijrmms.2011.09.005.
Goodman, R. E. (1969), The deformability of joints, paper presented at Determination of the in-situ modulus of deformation of rock, Amer. Soc. Test & Mats., STP 477, Denver, Colo.
Grasselli, G., J. Wirth, and P. Egger (2002), Quantitative three-dimensional description of a rough surface and parameter evolution with shearing, *Int. J. Rock Mech. Min. Sci.*, *39*(6), 789–800, doi:10.1016/S1365-1609(02)00070-9.
Haberfield, C. M., and I. W. Johnston (1994), A mechanistically-based model for rough rock joints, *Int. J. Rock Mech. Min. Sci.*, *31*(4), 279–292, doi:10.1016/0148-9062(94)90898-2.
Haberfield, C. M., and J. P. Seidel (1999), Some recent advances in the modelling of soft rock joints in direct shear, *Geotech. Geol. Eng.*, *17*(3–4), 177–195, doi:10.1023/A:1008900905076.
Hans, J., and M. Boulon (2003), A new device for investigating the hydro-mechanical properties of rock joints, *Int. J. Numer. Anal. Methods Geomech.*, *27*(6), 513–548. doi:10.1002/nag.285.
Haque, A. (1999), Shear behaviour of rock joints under constant normal stiffness, PhD thesis, Univ. of Wollongong, New South Wales, Australia.
Holditch, S. A., and R. A. Morse (1976), The effects of non-Darcy flow on the behavior of hydraulically fractured gas wells, *J. Pet. Technol.*, *28*(10), 1169–1179, doi:10.2118/5586-PA.
Holland, M., H. van Gent, L. Bazalgette, N. Yassir, E. H. Hoogerduijn Strating, and J. L. Urai (2011), Evolution of dilatant fracture networks in a normal fault—Evidence from 4D model experiments, *Earth Planet. Sci. Lett.*, *304*(3–4), 399–406, doi:10.1016/j.epsl.2011.02.017.
Huang, T. H., C. S. Chang, and C. Y. Chao (2002), Experimental and mathematical modeling for fracture of rock joint with regular asperities, *Eng. Fract. Mech.*, *69*(17), 1977–1996, doi:10.1016/S0013-7944(02)00072-3.

Huang, X., B. C. Haimson, M. E. Plesha, and X. Qiu (1993), An investigation of the mechanics of rock joints part I. Laboratory investigation, *Int. J. Rock Mech. Min. Sci.*, *30*(3), 257–269, doi:10.1016/0148-9062(93)92729-A.
Huitt, J. J. (1956), Fluid flow in simulated fractures, *AICHE J.*, *2*(2), 259–264, doi:10.1002/aic.690020224.
Isakov, E., S. R. Ogilvie, C. W. Taylor, and P. W. J. Glover (2001), Fluid flow through rough fractures in rocks I: High resolution aperture determinations, *Earth Planet. Sci. Lett.*, *191*(3–4), 267–282, doi:10.1016/S0012-821X(01)00424-1.
Javadi, M., M. Sharifzadeh, and K. Shahriar (2010), A new geometrical model for non-linear fluid flow through rough fractures, *J. Hydrol.*, *389*(1–2), 18–30, doi:10.1016/j.jhydrol.2010.05.010.
Ji, S.-H., H.-B. Lee, I. W. Yeo, and K.-K. Lee (2008), Effect of nonlinear flow on DNAPL migration in a rough-walled fracture, *Water Resour. Res.*, *44*, W11431, doi:10.1029/2007WR006712.
Jiang, Y., J. Xiao, Y. Tanabashi, and T. Mizokami (2004), Development of an automated servo-controlled direct shear apparatus applying a constant normal stiffness condition, *Int. J. Rock Mech. Min. Sci.*, *41*(2), 275–286, doi:10.1016/j.ijrmms.2003.08.004.
Jing, L., E. Nordlund, and O. Stephansson (1992), An experimental study on the anisotropy and stress-dependency of the strength and deformability of rock joints, *Int. J. Rock Mech. Min. Sci.*, *29*(6), 535–542, doi:10.1016/0148-9062(92)91611-8.
Jing, L., E. Nordlund, and O. Stephansson (1994), A 3-D constitutive model for rock joints with anisotropic friction and stress dependency in shear stiffness, *Int. J. Rock Mech. Min. Sci.*, *31*(2), 173–178, doi:10.1016/0148-9062(94)92808-8.
Jung, R. (1989), Hydraulic in situ investigations of an artificial fracture in the Falkenberg granite, *Int. J. Rock Mech. Min. Sci.*, *26*(3–4), 301–308, doi:10.1016/0148-9062(89)91978-5.
Karami, A., and D. Stead (2008), Asperity degradation and damage in the direct shear test: A hybrid FEM/DEM approach, *Rock Mech. Rock Eng.*, *41*(2), 229–266, doi:10.1007/s00603-007-0139-6.
Kohl, T., K. F. Evans, R. J. Hopkirk, R. Jung, and L. Rybach (1997), Observation and simulation of non-Darcian flow transients in fractured rock, *Water Resour. Res.*, *33*(3), 407–418, doi:10.1029/96WR03495.
Kolditz, O. (2001), Non-linear flow in fractured rock, *Int. J. Numer. Methods Heat Fluid Flow*, *11*(6), 547–575, doi:10.1108/EUM0000000005668.
Konzu, J. S., and B. H. Kueper (2004), Evaluation of cubic law based models describing single-phase flow through a rough-walled fracture, *Water Resour. Res.*, *40*, W02402, doi:10.1029/2003WR002356.
Koyama, T., N. Fardin, O. Stephansson, and L. Jing (2006), Numerical simulation of shear-induced flow anisotropy and scale-dependent aperture and transmissivity evolution of rock fracture replicas, *Int. J. Rock Mech. Min. Sci.*, *43*(1), 89–106, doi:10.1016/j.ijrmms.2005.04.006.
Koyama, T., B. Li, Y. Jiang, and L. Jing (2009), Numerical modelling of fluid flow tests in a rock fracture with a special algorithm for contact areas, *Comput. Geotech.*, *36*(1–2), 291–303, doi:10.1016/j.compgeo.2008.02.010.
Kwafniewski, M. A., and J. A. Wang (1997), Surface roughness evolution and mechanical behavior of rock joints under shear, *Int. J. Rock Mech. Min. Sci.*, *34*(3–4), 157.e1–157.e14, doi:10.1016/S1365-1609(97)00042-7.
Leichnitz, W. (1985), Mechanical properties of rock joints, *Int. J. Rock Mech. Min. Sci.*, *22*(5), 313–321, doi:10.1016/0148-9062(85)92063-7.
Li, B., Y. Jiang, T. Koyama, L. Jing, and Y. Tanabashi (2008), Experimental study of the hydro-mechanical behavior of rock joints using a parallel-plate model containing contact areas and artificial fractures, *Int. J. Rock Mech. Min. Sci.*, *45*(3), 362–375, doi:10.1016/j.ijrmms.2007.06.004.
Lomize, G. M. (1951), Filtratsia v treshchinovatykh porodakh (Seepage in Jointed Rocks), Gosudarstvennoe Energetitcheskoe Izdatel'stvo, Moskva-Leningrad.
Lopez, P., J. Riss, and G. Archambault (2003), An experimental method to link morphological properties of rock fracture surfaces to their mechanical properties, *Int. J. Rock Mech. Min. Sci.*, *40*(6), 947–954, doi:10.1016/S1365-1609(03)00052-2.
Louis, C. (1969), A study of groundwater flow in jointed rock and its influence on the stability of rock masses, *Rock Mech. Res. Rep. 10*, Imp. Coll., London.
Matsuki, K., Y. Chida, and K. Sakaguchi (2005), Anisotropic and heterogenous water flow in a sheared fracture as estimated in large synthetic fractures, *Trans. Geotherm. Resour. Counc.*, *29*, 401–406.
Matsuki, K., Y. Chida, K. Sakaguchi, and P. W. J. Glover (2006), Size effect on aperture and permeability of a fracture as estimated in large synthetic fractures, *Int. J. Rock Mech. Min. Sci.*, *43*, 726–755, doi:10.1016/j.ijrmms.2005.12.001.
Matsuki, K., Y. Kimura, K. Sakaguchi, A. Kizaki, and A. A. Giwelli (2010), Effect of shear displacement on the hydraulic conductivity of a fracture, *Int. J. Rock Mech. Min. Sci.*, *47*(3), 436–449, doi:10.1016/j.ijrmms.2009.10.002.
Mitani, Y., M. Sharifzadeh, T. Esaki, and F. Urakawa (2005), Development of shear-flow test apparatus and determination of coupled properties of rock joint, in *Proceeding of the Eurock 2005 – Impact of Human Activity on the Geological Environment*, pp. 397–403, A. A. Balkema, Leiden, Netherlands.
Moradian, Z. A., G. Ballivy, P. Rivard, C. Gravel, and B. Rousseau (2010), Evaluating damage during shear tests of rock joints using acoustic emissions, *Int. J. Rock Mech. Min. Sci.*, *47*, 590–598, doi:10.1016/j.ijrmms.2010.01.004.
Mourzenko, V. V., J.-F. Thovert, and P. M. Adler (1995), Permeability of a single fracture: Validity of the Reynolds equation, *J. Phys. II*, *5*(3), 465–482, doi:10.1051/jp2:1995133.
Moutsopoulos, K. N. (2009), Exact and approximate analytical solutions for unsteady fully developed turbulent flow in porous media and fractures for time dependent boundary conditions, *J. Hydrol.*, *369*(1–2), 78–89, doi:10.1016/j.jhydrol.2009.02.025.
Neuzil, C. E., and J. V. Tracy (1981), Flow through fractures, *Water Resour. Res.*, *17*(1), 191–199, doi:10.1029/WR017i001p00191.
Nicholl, M. J., H. Rajaram, R. J. Glass, and R. L. Detwiler (1999), Saturated flow in a single fracture: Evaluation of the Reynolds equation in measured aperture fields, *Water Resour. Res.*, *35*(11), 3361–3373, doi:10.1029/1999WR900241.
Nowamooz, A., G. Radilla, and M. Fourar (2009), Non-Darcian two-phase flow in a transparent replica of a rough-walled rock fracture, *Water Resour. Res.*, *45*, W07406, doi:10.1029/2008WR007315.
O'Brien, G. S., C. J. Bean, and F. McDermott (2003), Numerical investigations of passive and reactive flow through generic single fractures with heterogeneous permeability, *Earth Planet. Sci. Lett.*, *213*(3–4), 271–284, doi:10.1016/S0012-821X(03)00342-X.
Ogilvie, S. R., E. Isakov, and P. W. J. Glover (2006), Fluid flow through rough fractures in rocks. II: A new matching model for rough rock fractures, *Earth Planet. Sci. Lett.*, *241*(3–4), 454–465, doi:10.1016/j.epsl.2005.11.041.
Olsson, R., and N. Barton (2001), An improved model for hydromechanical coupling during shearing of rock joints, *Int. J. Rock Mech. Min. Sci.*, *38*(3), 317–329, doi:10.1016/S1365-1609(00)00079-4.
Olsson, W. A. (1992), The effect of slip on the flow of fluid through a fracture, *Geophys. Res. Lett.*, *19*(6), 541–543, doi:10.1029/92GL00197.
Olsson, W. A., and S. R. Brown (1993), Hydromechanical response of a fracture undergoing compression and shear, *Int. J. Rock Mech. Min. Sci.*, *30*(7), 845–851, doi:10.1016/0148-9062(93)90034-B.

Oron, A. P., and B. Berkowitz (1998), Flow in rock fractures: The local cubic law assumption reexamined, *Water Resour. Res.*, *34*(11), 2811–2825, doi:10.1029/98WR02285.
Park, J.-W., and J.-J. Song (2009), Numerical simulation of a direct shear test on a rock joint using a bonded-particle model, *Int. J. Rock Mech. Min. Sci.*, *46*(7), 1315–1328, doi:10.1016/j.ijrmms.2009.03.007.
Parrish, D. R. (1963), Fluid flow in rough fractures, paper presented at Production Research Symposium, Joint SPE-AIME, Univ. of Okla., Norman, Okla.
Pereira, J. P., and M. H. de Freitas (1993), Mechanisms of shear failure in artificial fractures of sandstone and their implication for models of hydromechanical coupling, *Rock Mech. Rock Eng.*, *26*(3), 195–214, doi:10.1007/BF01040115.
Pyrak-Nolte, L. J., N. G. W. Cook, and D. D. Nolte (1988), Fluid percolation through single fractures, *Geophys. Res. Lett.*, *15*(11), 1247–1250, doi:10.1029/GL015i011p01247.
Qian, J., H. Zhan, W. Zhao, and F. Sun (2005), Experimental study of turbulent unconfined groundwater flow in a single fracture, *J. Hydrol.*, *311*(1–4), 134–142, doi:10.1016/j.jhydrol.2005.01.013.
Qian, J., H. Zhan, Z. Chen, and H. Ye (2011), Experimental study of solute transport under non-Darcian flow in a single fracture, *J. Hydrol.*, *399*(3), 246–254, doi:10.1016/j.jhydrol.2011.01.003.
Quinn, P. M., J. A. Cherry, and B. L. Parker (2011), Quantification of non-Darcian flow observed during packer testing in fractured sedimentary rock, *Water Resour. Res.*, *47*, W09533, doi:10.1029/2010WR009681.
Ranjith, P. G., and W. Darlington (2007), Nonlinear single-phase flow in real rock joints, *Water Resour. Res.*, *43*, W09502, doi:10.1029/2006WR005457.
Ranjith, P. G., and D. R. Viete (2011), Applicability of the 'cubic law' for non-Darcian fracture flow, *J. Pet. Sci. Eng.*, *78*(2), 321–327, doi:10.1016/j.petrol.2011.07.015.
Renshaw, C. E. (1995), On the relationship between mechanical and hydraulic apertures in rough-walled fractures, *J. Geophys. Res.*, *100*(B12), 629–636, doi:10.1029/95JB02159.
Ruina, A. (1983), Slip instability and state variable friction laws, *J. Geophys. Res.*, *88*(B12), 10,359–10,370, doi:10.1029/JB088iB12p10359.
Ruth, D., and H. Ma (1992), On the derivation of the Forchheimer equation by means of the averaging theorem, *Transp. Porous Media*, *7*(3), 255–264, doi:10.1007/BF01063962.
Saeb, S., and B. Amadei (1992), Modelling rock joints under shear and normal loading, *Int. J. Rock Mech. Min. Sci.*, *29*(3), 267–278, doi:10.1016/0148-9062(92)93660-C.
Schrauf, T. W., and D. D. Evans (1986), Laboratory studies of gas flow through a single natural fracture, *Water Resour. Res.*, *22*(7), 1038–1050, doi:10.1029/WR022i007p01038.
Seidel, J. P., and C. M. Haberfield (2002), A theoretical model for rock joints subjected to constant normal stiffness direct shear, *Int. J. Rock Mech. Min. Sci.*, *39*(5), 539–553, doi:10.1016/S1365-1609(02)00056-4.
Sharifzadeh, M. (2005), Experimental and theoretical research on hydro-mechanical coupling properties of rock joint, PhD thesis, Dep. of Civ. and Struct. Eng., Kyushu Univ., Fukuoka, Japan.
Sharifzadeh, M., Y. Mitani, and T. Esaki (2006), Rock joint surfaces measurement and analysis of aperture distribution under different normal and shear loading using GIS, *Rock Mech. Rock Eng.*, *41*(2), 299–323, doi:10.1007/s00603-006-0115-6.
Skjetne, E., A. Hansen, and J. S. Gudmundsson (1999), High-velocity flow in a rough fracture, *J. Fluid Mech.*, *383*, 1–28, doi:10.1017/S0022112098002444.
Sun, Z., C. Gerrard, and O. Stephansson (1985), Rock joint compliance tests compression for and shear loads, *Int. J. Rock Mech. Min. Sci.*, *22*(4), 197–213, doi:10.1016/0148-9062(85)92948-1.
Talon, L., H. Auradou, and A. Hansen (2010), Permeability of self-affine aperture fields, *Phys. Rev. E*, *82*(4), 046108, doi:10.1103/PhysRevE.82.046108.
Tsang, Y. W. (1984), The effect of tortuosity on fluid-flow through a single fracture, *Water Resour. Res.*, *20*(9), 1209–1215, doi:10.1029/WR020i009p01209.
Tsang, Y. W., and C. F. Tsang (1987), Channel model of flow through fractured media, *Water Resour. Res.*, *23*(3), 467–479, doi:10.1029/WR023i003p00467.
Tsang, Y. W., and P. A. Witherspoon (1981), Hydromechanical behavior of a deformable rock fracture subject to normal stress, *J. Geophys. Res.*, *86*(B10), 9287–9298, doi:10.1029/JB086iB10p09287.
Watanabe, N., N. Hirano, and N. Tsuchiya (2008), Determination of aperture structure and fluid flow in a rock fracture by high-resolution numerical modeling on the basis of a flow-through experiment under confining pressure, *Water Resour. Res.*, *44*, W06412, doi:10.1029/2006WR005411.
Wen, Z., G. Huang, and H. Zhan (2006), Non-Darcian flow in a single confined vertical fracture toward a well, *J. Hydrol.*, *330*(3–4), 698–708, doi:10.1016/j.jhydrol.2006.05.001.
Witherspoon, P. A., J. S. Y. Wang, K. Iwai, and J. E. Gale (1980), Validity of cubic law for fluid flow in a deformable rock fracture, *Water Resour. Res.*, *16*(6), 1016–1024, doi:10.1029/WR016i006p01016.
Xiong, X., B. Li, Y. Jiang, T. Koyama, and C. Zhang (2011), Experimental and numerical study of the geometrical and hydraulic characteristics of a single rock fracture during shear, *Int. J. Rock Mech. Min. Sci.*, *48*(8), 1292–1302, doi:10.1016/j.ijrmms.2011.09.009.
Yeo, I. W., and S. Ge (2001), Solute dispersion in rock fractures by non-Darcian flow, *Geophys. Res. Lett.*, *28*(20), 3983–3986, doi:10.1029/2001GL013274.
Yeo, I. W., M. H. de Freitas, and R. W. Zimmerman (1998), Effect of shear displacement on the aperture and permeability of a rock fracture, *Int. J. Rock Mech. Min. Sci.*, *35*(8), 1051–1070, doi:10.1016/S0148-9062(98)00165-X.
Zeng, Z., and R. Grigg (2006), A criterion for non-Darcy flow in porous media, *Transp. Porous Media*, *63*(1), 57–69, doi:10.1007/s11242-005-2720-3.
Zhang, H. Q., Z. Y. Zhao, C. A. Tang, and L. Song (2006), Numerical study of shear behavior of intermittent rock joints with different geometrical parameters, *Int. J. Rock Mech. Min. Sci.*, *43*(5), 802–816, doi:10.1016/j.ijrmms.2005.12.006.
Zhao, J. (1997), Joint surface matching and shear strength part B: JRC-JMC shear strength criterion, *Int. J. Rock Mech. Min. Sci.*, *34*(2), 179–185, doi:10.1016/S0148-9062(96)00063-0.
Zimmerman, R. W., and G. S. Bodvarsson (1996), Hydraulic conductivity of rock fractures, *Transp. Porous Media*, *23*(1), 1–30, doi:10.1007/BF00145263.
Zimmerman, R. W., A. H. Al-Yaarubi, C. C. Pain, and C. A. Grattoni (2004), Non-linear regimes of fluid flow in rock fractures, *Int. J. Rock Mech. Min. Sci.*, *41*(3), 163–169, doi:10.1016/j.ijrmms.2003.12.045.